NASA TN D-90

TECHNICAL NOTE
D-90

A STUDY OF METHODS FOR SIMULATING THE ATMOSPHERE ENTRY OF VEHICLES WITH SMALL-SCALE MODELS

By Byron L. Swenson

Ames Research Center
Moffett Field, Calif.

NATIONAL AERONAUTICS AND SPACE ADMINISTRATION
WASHINGTON

April 1960

NATIONAL AERONAUTICS AND SPACE ADMINISTRATION

TECHNICAL NOTE D-90

A STUDY OF METHODS FOR SIMULATING THE ATMOSPHERE ENTRY OF VEHICLES WITH SMALL-SCALE MODELS

By Byron L. Swenson

SUMMARY

It is demonstrated by a motion and aerodynamic heating analysis of various types of lifting and nonlifting satellite entries that the heating-rate histories may be represented approximately by one curve if they are properly made dimensionless. Attention is then focused on a study of the simulation of critical thermal effects on satellite vehicles with particular attention to the use of small-scale models. The generalized heating-rate history shows that simulation of heating effects in lifting and nonlifting satellites can be accomplished with properly designed small-scale ballistic models. It is also shown that an atmosphere-entry simulator designed primarily for the testing of ballistic vehicles may be used to advantage for the simulation of effects in lifting and nonlifting satellites. Similarity relations are derived and an application of these relations is made to the simulation of heating effects on a lifting satellite vehicle.

A study is also presented of the possibility of firing a model upstream in an atmosphere-entry simulator with a high stream velocity to obtain the high stagnation enthalpies of entry from highly elliptic, parabolic, and hyperbolic trajectories.

INTRODUCTION

The aerodynamic heating experienced by recoverable space and satellite vehicles during an atmosphere entry poses an important problem to the designer. Since full-scale tests of these vehicles are costly and time-consuming, it is proper to determine whether simulation of the heating effects is possible with properly designed small-scale models flown along appropriate trajectories. There is also the attractive possibility of using relatively simple equipment on the ground, such as an atmosphere-entry simulator originally designed for ballistic missiles (see ref. 1), for the simulation of these effects in recoverable satellite and space vehicles.

Simulation is usually accomplished by a proper scaling of the heating-rate history and a consistent scaling of the particular critical

quantity (as for example, thermal stress) to be simulated. With this fact in mind, this paper undertakes first to establish the motion and heating of vehicles of this type, and then to establish relations of similarity for the various effects of this heating.

ANALYSIS

Motion

In the consideration of the heating experienced by a vehicle entering the earth's atmosphere, it is first necessary to determine the operating conditions that it will experience. These conditions are dictated by the vehicle's motion through the atmosphere and it is therefore necessary first to make an analysis of this motion. The reader is directed to the numerous analyses of this type, such as references 2, 3, 4, and 5. For the purposes of this paper an analysis such as found in reference 2 will be used.

For the purposes of future identification, the three classes of vehicles considered in this report will be identified as follows:

1. Lifting satellites: Vehicles capable of using some lift during entry from a satellite orbit. Entry is initiated at satellite speed and at a very small angle to the horizontal.

2. Nonlifting satellites: Nonlifting vehicles which initiate entry at satellite speed and at a very small angle to the horizontal.

3. Ballistic vehicles: Nonlifting configurations which initiate entry at somewhat lower than satellite speed and at a large or moderate angle to the horizontal (i.e., entry at angles of approximately 20° or more).

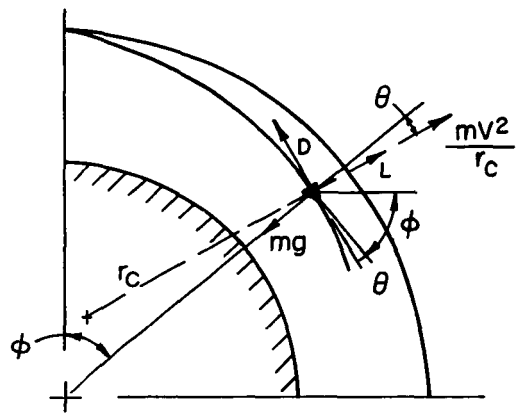

Sketch (a)

In general, a vehicle during entry is subjected to aerodynamic, centrifugal, and gravitational forces as shown in sketch (a). The parametric equations of motion along and normal to the flight path can be written as:

$$mg \sin \theta - D = m \frac{dV}{dt} \qquad (1)$$

$$mg \cos \theta - L = m \frac{V^2}{r_c} \qquad (2)$$

where r_c is the local radius of curvature of the flight path and θ is the angle of the flight path to the local horizontal, measured positive downward. All symbols are defined in appendix A.

We now focus our attention on the two types of entry trajectories which will be of interest to us, namely, (1) the satellite entry (lifting and nonlifting) and (2) the ballistic entry. The satellite entry is characterized by entry at satellite speed at a small inclination such that $|\theta| \ll 1$ throughout the trajectory except in the terminal phase, and the ballistic entry is characterized by entry at large angles with a resultant small flight-path curvature or an essentially straight-line trajectory (see ref. 3).

Eggers (ref. 2) has shown that for satellite entry ($|\theta| \ll 1$, $|mg\theta| \ll D$) into an isothermal atmosphere (i.e., $\rho = \rho_o e^{-\beta y}$) equations (1) and (2) can be combined, for the case of constant C_D and L/D, into the following single differential equation of motion:

$$f \frac{d^2 f}{dz^2} + Kf + (1 - e^{-z}) = 0 \tag{3}$$

where

$$f = \frac{C_D \rho_o A}{m} \sqrt{\frac{r_o}{\beta}}\, e^{-\beta y} \tag{4}$$

$$z = \ln \frac{V^2}{g r_o} = \ln \frac{V^2}{V_{sat}^2} \tag{5}$$

$$K = \frac{L}{D} \frac{\sqrt{\beta r_o}}{2} \tag{6}$$

It can be seen that f and z are transformed altitude and velocity coordinates and that K is an L/D parameter.

In the large-angle ballistic trajectory, forces normal to the flight path play a very small part in the determination of the motion of the entering vehicle. The flight path becomes essentially a straight line. The trajectory can then be represented by the single equation of motion along the flight path, again neglecting the component of weight along the flight path in comparison to the drag. If it is noted that $dy/dt = -V \sin \theta_E$, and if the isothermal atmosphere is assumed,

equation (1) yields:

$$\frac{C_D \rho_o A}{2m} V^2 e^{-\beta y} = V \sin \theta_E \frac{dV}{dy} \tag{7}$$

where θ_E is the entrance angle, constant throughout entry. Use of the coordinate transforms defined by equations (4) and (5) yields the following differential equation of motion for a large-angle ballistic entry:

$$\frac{df}{dz} = -\sqrt{\beta r_o} \sin \theta_E \tag{8}$$

Heating

Before we consider the solution of the differential equations of motion, let us first consider some general aspects of the aerodynamic heating of vehicles of this type.

The stagnation-point heating rate under the conditions of laminar incompressible flow with a Prandtl number of unity is given by (see refs. 3 and 6)

$$q_s = C \sqrt{\frac{\rho}{\sigma}} V^3 \tag{9}$$

where C is constant and σ is the stagnation-point radius of curvature. Rewriting equation (9) in the f and z coordinates yields (for an isothermal atmosphere)

$$q_s = C' f^{1/2} e^{(3/2)z} \tag{10}$$

where

$$C' = C V_{sat}^3 \sqrt[4]{\frac{\beta}{r_o}} \left(\frac{m}{C_D A \sigma} \right)^{1/2} \tag{10a}$$

Differentiating equation (10) to determine the maximum stagnation-point heating rate and the f and z coordinates of the trajectory point where this heating rate occurs yields:

$$\left(\frac{df}{dz}\right)^* + 3f^* = 0 \tag{11}$$

where the asterisk refers to the trajectory point corresponding to the maximum stagnation-point heating rate.

For the purpose of simulation of thermal effects on the entering vehicle, it is necessary to consider the time history of the heating rates and the integrated heat input to the structure. The trajectory can be determined chronologically with respect to the altitude and velocity coordinates for both satellite and ballistic entries from equation (1), written in the form

$$\frac{dV}{dt} = -\frac{C_D \rho_o A}{2m} V^2 e^{-\beta y} \tag{12}$$

or written in the f-z coordinates as:

$$\sqrt{\beta g}\, dt = -\frac{dz}{f e^{z/2}} \tag{13}$$

If time is measured from the instant of maximum stagnation-point heating rate (i.e., $t = 0$ at $z = z^*$), we obtain:

$$t = -\frac{1}{\sqrt{\beta g}} \int_{z^*}^{z} \frac{dz}{f e^{z/2}} \tag{14}$$

Using equations (10), (11), and (14) we may now present the heating-rate history parametrically in terms of the velocity coordinate z in the following dimensionless form:

$$\frac{q_s}{q_s{}^*} = \bar{q}_s = \left(\frac{f}{f^*}\right)^{1/2} e^{3/2(z-z^*)} \tag{15}$$

$$\frac{t}{t_o} = \bar{t} = -\frac{1}{t_o\sqrt{\beta g}} \int_{z^*}^{z} \frac{dz}{f e^{z/2}} \tag{16}$$

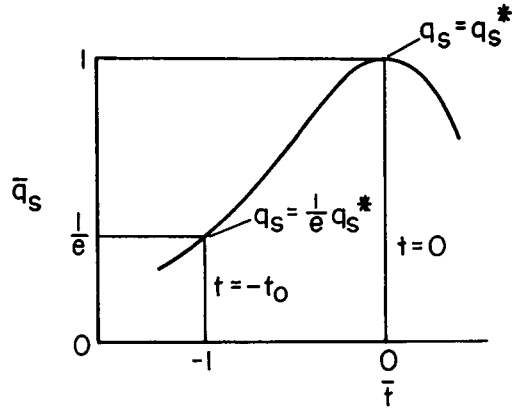

Sketch (b)

where time is made dimensionless in such a way that $\bar{t} = -1$ when $\bar{q}_s$ assumes the value $1/e$ on the high velocity side of the heating pulse. The choice of this value is somewhat arbitrary. For clarity, the scheme for making the heating-rate history dimensionless is shown in sketch (b). The trajectory function $f = f(z)$ is determined from the differential equation of motion, and the starred conditions are determined from the motion equation together with equation (11).

Note that the advantage of defining the heating-rate history in this way is that two points of the history are the same for all trajectories (i.e., $\bar{q}_s = 1/e$ at $\bar{t} = -1$ and $\bar{q}_s = 1$ at $\bar{t} = 0$).

This analysis has been for laminar flow in the stagnation region of the nose. An analysis for the aerodynamic heating experienced by other points on the body, under the condition of turbulent flow, can be made in a similar manner starting from equation (B7), derived in appendix B, instead of equation (9).

Trajectory

The solution of the equation of motion for satellite entries is complicated by the nonlinearity of equation (3). As a first approximation let us consider equilibrium gliding flight in which the lift plus centrifugal force balances the weight. Under these conditions equation (3) reduces to the algebraic equation relating flight altitude to flight velocity,

$$f = \frac{e^{-z} - 1}{K} \tag{17}$$

Equation (17) is a very tractable equation and its application to the study of the gross motions of lifting satellites is shown in figure 1.

Here equilibrium glide is shown in comparison to a high-speed digital machine computation of equation (3) for an example L/D of 0.5. Note that the numerical solution to equation (3) skips around the equilibrium-glide trajectory, but as far as the gross motion of the vehicle is concerned, the equilibrium-glide trajectory is adequate for the purposes of this paper.

Under the nonlifting condition (i.e., K = 0), equation (3) becomes

$$f \frac{d^2 f}{dz^2} = e^{-z} - 1$$

Eggers (ref. 2) has shown that a sufficiently accurate solution for this case is the following:

$$f = - \frac{1}{\sqrt{k}} z \left(1 - \frac{k}{2} z \right) \tag{18}$$

where

$$k = \frac{1}{\beta r_o \theta_E^2}$$

and should be of the order of 1 or less. For the planet Earth, this condition means θ_E must be of the order of 2° or more.

The solution of the equation of motion for large-angle ballistic entries is comparatively simple. Under the boundary condition that at $f = 0$ (i.e., $y \to \infty$), $z = z_E$, equation (8) integrates to give

$$f = - \sqrt{\beta r_o} \sin \theta_E (z_E - z) \tag{19}$$

We have thus determined trajectory relationships for each of the three types of atmosphere entries under consideration.

Heating History

We are now in a position to determine the operating conditions for these trajectories. For the case of the equilibrium-glide trajectory the

dimensionless heating-rate history can be determined from equations (11), (15), (16), and (17),

$$\left.\begin{aligned} \bar{q}_s &= 2.598 e^{(3/2)z}(e^{-z} - 1)^{1/2} \\ \bar{t} &= \frac{K}{(t_o)_{ls}\sqrt{\beta g}} \ln\left[-9.90 \tanh\left(\frac{z}{4}\right)\right] \end{aligned}\right\} \tag{20}$$

where

$$(t_o)_{ls} = \frac{K}{\sqrt{\beta g}} 2.950 \qquad \text{(lifting satellite time constant)} \tag{20a}$$

The maximum heating rate for this case is determined from equations (10), (11), and (17) as the following:

$$(q_s^*)_{ls} = \frac{2\sqrt{3}}{9} \frac{C'_{ls}}{K^{1/2}} \tag{21}$$

where

$$z^* = \ln \frac{2}{3}$$

In a similar way, the heating-rate history may be determined for the nonlifting satellite trajectory from equations (11), (15), (16), and (18). The maximum heating rate is determined from equations (10), (11), and (18). As an example k will be assumed as unity (see eq. (18)). For this case, the heating-rate history and maximum heating rate are:

$$\left.\begin{aligned} \bar{q}_s &= 2.630e^{(3/2)z}\left(\frac{z^2}{2} - z\right)^{1/2} \\ \bar{t} &= \frac{1}{(t_o)_{ns}\sqrt{\beta g}}\left\{\ln\left(\frac{-z}{0.389}\right) + \sum_{n=1}^{\infty}\frac{(-z/2)^n}{n \cdot n!}\right. \\ &\quad \left. - \frac{1}{e}\ln\left[-\frac{(z/2)-1}{1.195}\right] - \frac{1}{e}\sum_{n=1}^{\infty}\frac{[1-(z/2)]^n}{n \cdot n!} + 0.4155\right\} \end{aligned}\right\} \qquad (22)$$

A
3
2
3

where

$$(t_o)_{ns} = \frac{3.210}{\sqrt{\beta g}} \qquad \text{(nonlifting satellite time constant)} \qquad (22a)$$

and

$$(q_s^*)_{ns} = 0.3805C'_{ns} \qquad (23)$$

where

$$z^* = -0.389$$

The large-angle ballistic heating-rate history and maximum heating rate are determined in a similar way using equation (19) for the trajectory function. The results are as follows:

$$\left.\begin{aligned} \bar{q}_s &= [3(z_E - z)]^{1/2} e^{(3/2)[(1/3)-(z_E-z)]} \\ \bar{t} &= \frac{1}{(t_o)_b \beta V_E \sin\theta_E}\left\{\ln[3(z_E-z)] + \sum_{n=1}^{\infty}\frac{1}{2^n n \cdot n!}\left[(z_E-z)^n - \left(\frac{1}{3}\right)^n\right]\right\} \end{aligned}\right\} \qquad (24)$$

where

$$(t_o)_b = \frac{3.116}{\beta V_E \sin \theta_E} \qquad \text{(ballistic time constant)} \qquad (24a)$$

and

$$(q_s^*)_b = \left(\frac{1}{3e}\right)^{1/2} \left(\sqrt{\beta r_o}\, \sin \theta_E\right)_b^{1/2} C_b' \left(\frac{V_E}{V_{sat}}\right)_b^3 \qquad (25)$$

where

$$z^* - z_E = -\frac{1}{3}$$

The heating-rate histories for these three cases are shown in figure 2. Notice all the curves are forced through the two matching points (A) and (B), and when they are plotted in this form, all have essentially the same heating history up to and slightly beyond the maximum heating point. Therefore an approximate generalized heating history for these three trajectories can be represented by any one of equations (20), (22), or (24).

Atmosphere Entry Simulator

The preceding is an analysis of the motion and heating of satellite and ballistic entries into the earth's atmosphere. In reference 1, it is shown that a ballistic entry can be simulated on the ground in a device called an atmosphere-entry simulator. Later in this paper, the possibility of using the atmosphere-entry simulator to simulate not only ballistic entries, but lifting and nonlifting satellite entries, parabolic entries, and hyperbolic entries will be considered.

The atmosphere-entry simulator is described in detail in reference 1. It consists of a contoured supersonic nozzle which gives an exponential density distribution (i.e., $\rho = \rho_o e^{-\beta y}$) into which a model is fired upstream. The model is a ballistic configuration and flies down the center line of the nozzle. The air-stream velocity is assumed to be negligible in comparison to the model flight speed. The equation of motion is then given by:

$$\frac{C_D A}{m} \frac{\rho_o}{2} V^2 e^{-\beta y} = V \frac{dV}{dy}$$

This differential equation is the same as equation (7) with $\sin \theta_E = 1$. The values of β and y will be grossly different from those that exist in the earth's atmosphere, but at simulated trajectory points, the product βy will be the same for model and full-scale vehicle. This allows simulation of ballistic entries for a fixed altitude range and a wide range of entrance angles.

The heating-rate history equations (24) derived for the ballistic entry will now also hold for the simulator model with the exception that $\beta \sin \theta_E$ is different.

When the simulation of an atmosphere entry is considered from a parabolic or hyperbolic trajectory ($V_E \geq 36{,}000$ ft/sec), it is found that in order to duplicate the entrance velocity (hence enthalpy) in an atmosphere-entry simulator, it is convenient to use a high-stream velocity in conjunction with a high launching velocity of the model to give a relative velocity of the required magnitude. An analysis of the motion and heating of a model in this type of simulator is given in appendix C.

SIMULATION

We have now determined the operating conditions experienced by vehicles or models entering the earth's atmosphere along different trajectories. We have also examined the conditions that a model fired in an atmosphere-entry simulator will experience. In this section, we shall proceed to examine these conditions to establish whether simulation of heating effects is possible by testing small-scale models.

Before we look into the problem of the simulation of heating effects on vehicles entering the earth's atmosphere, let us first consider some of the types of heat shielding designs and the possible critical design considerations of each.

There are primarily three types of heat shielding designs now being considered: (1) the heat-sink design, (2) the radiation-shield design, and (3) the ablation-cooled design. Although combinations of these types may be desirable in certain cases, this paper will be concerned with the simulation of heating effects for the three separate types only.

When simulation is considered, the obvious question is what parameter should be simulated. Generally, it is not possible to simulate entirely a given system with a single small-scale test. It is therefore necessary to make some evaluation of what is the most important parameter in a given system which should be duplicated, and to scale the model and environment accordingly. For example, in a heat-sink design, thermal stress may be considered as a major design parameter, while in a radiation-shield design, with a thin nonload-carrying structure, thermal stress may be replaced by actual surface temperature as a major design parameter. In an

ablation-cooled design, the effectiveness of the ablating material in protecting a vehicle from severe heating rates may be of prime importance. With these thoughts in mind, we shall now focus our attention on each of these designs separately to determine whether the suggested parameters can be simulated. If other parameters are considered more important, a method similar to that presented in this paper may be used to derive the similarity relations necessary for simulation.

Heat Sink

Ballistic vehicles.- The simulation of thermal stress in the heat-sink material of ballistic vehicles has been examined thoroughly by Eggers in reference 1.

Lifting satellite.- The general conditions to be matched for simulation of thermal stress in the heat-sink material between model and full-scale vehicle are (from ref. 1):

$$\left(\frac{Q}{m}\right)_m = \left(\frac{Q}{m}\right)_f \tag{26}$$

$$q_m = \frac{1}{\lambda} q_f \tag{27}$$

and

$$Re_m = Re_f$$

where the subscripts m and f indicate model and full scale, respectively; λ is the model to vehicle scale factor; Q/m is the total heat absorbed per unit mass of heat-sink material; and Re is the Reynolds number. If we restrict ourselves to using the same material in the model heat sink as in the full-scale vehicle heat sink, equation (26) along with equation (27) reduces to the following time condition:

$$t_m = \lambda^2 t_f \tag{28}$$

In general, it is not possible to satisfy both equations (27) and (28) simultaneously throughout the entry trajectory without altering one or more of the basic vehicle parameters in the model. In order to derive

similarity relations by which we may design models that will simulate thermal stress, we shall use the following procedure. In figure 2, equation (28) will be matched at point (A) and equation (27) will be matched at point (B) of the generalized heating history. Equations (27) and (28) then take on the following form:

$$q_{s_m}{}^* = \frac{1}{\lambda} q_{s_f}{}^* \tag{29}$$

$$t_{o_m} = \lambda^2 t_{o_f} \tag{30}$$

The matching of heating-rate histories according to equations (29) and (30) completely determines the vehicle parameters of the model. In general, then, it is not possible to match the Reynolds number condition, but relaxing this condition slightly should not affect simulation so long as laminar flow exists at the stagnation region.

Consider first the low L/D glider utilizing a heat-sink design. By means of equations (10a) and (21) the maximum heating rate is obtained as:

$$(q_s{}^*)_{ls} = \frac{2\sqrt{6}}{9} \frac{C V_{sat}^3}{\sqrt{r_o}} \left(\frac{m}{C_L A \sigma}\right)^{1/2} \tag{31}$$

and equations (6) and (20a) yield the lifting satellite time constant as:

$$(t_o)_{ls} = 2.950 \left(\frac{1}{2} \frac{L}{D} \sqrt{\frac{r_o}{g}}\right) \tag{32}$$

It can be seen from equation (31) that the only vehicle parameter that may be varied in the small-scale model in order to obtain the higher heating rates dictated by equation (29) is $m/A\sigma$. This parameter is independent of scale factor but may be varied by changing the over-all density of the model. However, examination of equation (32) shows that the time condition (eq. (30)) can not be satisfied in any way. Thus we conclude that simulation of thermal-stress effects in lifting satellite vehicles is not possible by simple scale-model tests.

Since it has been shown that the heating-rate histories are approximately the same for different vehicles when the histories are

matched at the two aforementioned points, it may be possible to derive similarity relations between a lifting vehicle and a ballistic model. It would then be possible to simulate thermal-stress effects in lifting vehicles by use of an equivalent ballistic model.

Since most of the heating experienced by a lifting vehicle occurs on the high pressure region of the lower surface, an equivalent ballistic configuration could be designed by replacing the upper (low pressure) surface with a mirror image of the lower surface, thus forming a symmetrical body. Sketch (c) shows a lifting vehicle configuration and the symmetrical ballistic model of this configuration.

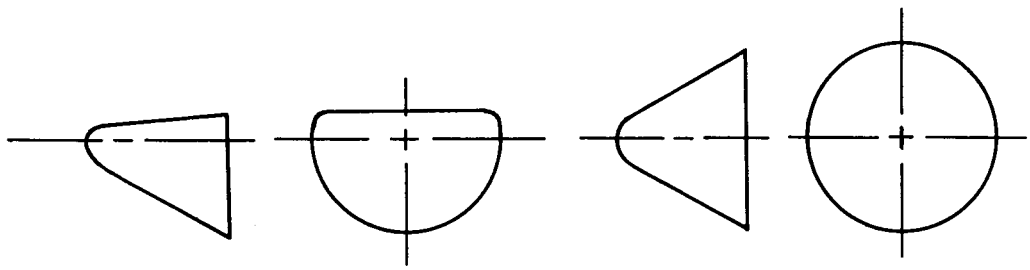

Sketch (c)

Matching the maximum heating rate of the small-scale ballistic configuration to the maximum heating rate of the glider according to equation (29) (squared for convenience) yields

$$\left(\frac{m\beta V_E^6 \sin\theta_E}{C_D A\sigma}\right)_b = \frac{1}{\lambda^2}\frac{8}{9}e\left(\frac{mV_{sat}^6}{r_o C_L A\sigma}\right)_{ls} \tag{33}$$

Matching the time condition according to equation (30) yields

$$\frac{3.116}{(\beta V_E \sin\theta_E)_b} = \lambda^2 2.950\left(\frac{1}{2}\frac{r_o}{V_{sat}}\frac{L}{D}\right)_{ls} \tag{34}$$

Equations (33) and (34) relate the vehicle and trajectory parameters of a small-scale ballistic model to those of a full-scale glider, each suffering approximately the same thermal stress during entry.

Since the ballistic model has two surfaces representing the lower surface of the lifting vehicle, we may write the following relations:

$$\left.\begin{aligned} m_b &= 2\eta\lambda^3 m_{ls} \\ (C_DA)_b &= 2\lambda^2 (C_DA)_{ls} \\ \sigma_b &= \lambda\sigma_{ls} \end{aligned}\right\} \tag{35}$$

where η is the ratio of over-all model density to over-all vehicle density. Substituting equations (35) into equation (33) and solving equations (33) and (34) for the required density scale factor for simulation yields:

$$\eta = \frac{2.950}{3.116} \frac{(4/9)e}{(V_{E_b}/V_{sat})^5} \tag{36}$$

The required model scale for the ballistic model can be found from equation (34).

$$\lambda^2 = \frac{3.116}{2.950} \left[\frac{2(V_{sat}/V_{E_b})}{\beta_b \sin\theta_{E_b} r_o (L/D)}\right] \tag{37}$$

The curve designated "Lifting satellite" in figure 3 shows the density scale factor η as a function of the ballistic entrance velocity. From equation (36) note that the density scale factor for simulation is independent of the size scale factor. The curve designated "Nonlifting satellite" will be discussed later.

Figure 4 is a plot of equation (37) showing the scale factor λ as a function of the ballistic entrance velocity for a glide vehicle with $L/D = 1.0$. Various values of the parameter $\beta_b \sin\theta_{E_b}$ are shown. These values range from that for the Ames Atmosphere-Entry Simulator ($0.15\ ft^{-1}$) to a typical value for atmosphere testing ($4.5\times10^{-5}\ ft^{-1}$).

We have now enough information about the scale factor and over-all weight to design ballistic models which may be boosted and made to re-enter the earth's atmosphere, or may be fired in an atmosphere-entry simulator. The thermal stress in the heat shield of these ballistic models will duplicate that of a lifting-satellite heat shield within the limits of the approximations and assumptions made.

Nonlifting satellite.- Consider now a nonlifting-type satellite utilizing a heat sink. The necessary conditions for simulation are again given by equations (29) and (30).

From equations (10a) and (23) the maximum heating rate is obtained as:

$$(q_s^*)_{ns} = 0.3805 C V_{sat}^3 \sqrt[4]{\frac{\beta_{ns}}{r_o}} \left(\frac{m}{C_D A \sigma}\right)_{ns}^{1/2} \tag{38}$$

and from equation (22a) the time constant is obtained as:

$$(t_o)_{ns} = \frac{3.210}{\sqrt{\beta_{ns} g}} \tag{39}$$

It can be seen from equations (38) and (39) that a change in the density of the model will not satisfy both equations (29) and (30). Therefore a small-scale model flying a nonlifting satellite trajectory can not be made to satisfy the conditions of simulation.

As before, let us now consider designing a ballistic model which will simulate the thermal stress effects on a nonlifting satellite. Matching the maximum heating rates as before, we obtain

$$\left(\frac{m\beta V_E^6 \sin \theta_E}{C_D A \sigma}\right)_b = \frac{0.434 e}{\lambda^2} \left(\frac{m V_{sat}^6 \sqrt{\beta / r_o}}{C_D A \sigma}\right)_{ns} \tag{40}$$

Matching the time condition according to equation (30) yields

$$\frac{3.116}{(\beta V_E \sin \theta_E)_b} = \lambda^2 \frac{3.210}{(\sqrt{\beta_{ns}/r_o}\, V_{sat})_{ns}} \tag{41}$$

Since the ballistic model and nonlifting satellite are similar in every respect except in over-all density (however, heat-sink materials must remain the same), we may write:

$$\left.\begin{aligned} m_b &= \eta\lambda^3 m_{ns} \\ (C_D A)_b &= \lambda^2 (C_D A)_{ns} \\ \sigma_b &= \lambda \sigma_{ns} \end{aligned}\right\} \qquad (42)$$

where η is the ratio of over-all model density to over-all vehicle density. Substituting equations (42) into equation (40) and solving equations (40) and (41) for the required density ratio for simulation yields

$$\eta = \frac{3.210}{3.116} \frac{0.434e}{(V_{E_b}/V_{sat})^5} \qquad (43)$$

The required scale factor for the ballistic model is determined from equation (41).

$$\lambda^2 = \frac{3.116}{3.210} \frac{V_{sat}}{V_{E_b}} \frac{\sqrt{\beta_{ns}/r_o}}{\beta_b \sin \theta_{E_b}} \qquad (44)$$

The scale factor is thus seen to depend on the entrance velocity.

The curve designated "Nonlifting satellite" in figure 3 is a plot of equation (43) showing the density scale factor η as a function of the ballistic entrance velocity. Note this curve is very similar to equation (36) for lifting satellites.

Figure 5 shows the scale factor λ as a function of ballistic entrance velocity. The various values of the parameter $\beta_b \sin \theta_{E_b}$ range again from the value for the Ames Atmosphere-Entry Simulator (0.15 ft^{-1}) to a typical value for atmosphere testing (4.5×10^{-5} ft^{-1}).

Equations (43) and (44) now give us sufficient information so that ballistic models may be designed which may be used in either an atmosphere test or an entry simulator test to simulate thermal stress effects in the heat sinks of nonlifting satellites.

Radiation Shield

Generally, the application of the radiation-shield design is most suitable for lifting vehicles because of the rather high peak radiation-equilibrium temperatures which would be experienced along other trajectories. For this reason we shall consider only simulation conditions for lifting satellites.

Because of the nature of the radiation-shield structure (i.e., thin nonload carrying) thermal stress may not be of critical importance. A more probable choice of the critical design parameter may be the radiation-equilibrium temperature of the surface. If this is the case, the surface-temperature history must be duplicated as closely as possible.

Assuming that after equilibrium is reached, all the heat transferred to the vehicle is radiated away, the conditions for simulation of surface temperature are then:

$$\left(\frac{q}{\epsilon}\right)_m = \left(\frac{q}{\epsilon}\right)_f \tag{45}$$

$$t_m = t_f \tag{46}$$

where ϵ is the surface emissivity.

Again the conditions of simulation will be matched at two points on the heating-rate history. Equation (46) will be matched at point (A) and equation (45) will be matched at point (B) in figure 2. Thus the conditions for simulation become:

$$\left(\frac{q_s^*}{\epsilon}\right)_m = \left(\frac{q_s^*}{\epsilon}\right)_f \tag{47}$$

$$(t_o)_m = (t_o)_f \tag{48}$$

From equations (31) and (32) it can be seen that if the model is exactly similar to the full-scale vehicle and has the same material in the radiation shield (i.e., $\epsilon_m = \epsilon_f$), then equations (47) and (48) are automatically satisfied and simulation is possible at any scale.

Let us now inquire as to the possibility of designing a ballistic model to simulate radiation-equilibrium temperatures of the glider. Equations (25) and (31) may be used to write equation (47) as:

$$\left(\frac{m\beta V_E^6 \sin\theta_E}{\epsilon^2 C_D A\sigma}\right)_b = \frac{8}{9} e \left(\frac{mV_{sat}^6}{\epsilon^2 r_o C_L A\sigma}\right)_{ls} \tag{49}$$

and from equations (24a) and (32), equation (48) becomes

$$\left(\frac{3.116}{\beta V_E \sin\theta_E}\right)_b = 2.950 \left(\frac{1}{2}\frac{r_o}{V_{sat}}\frac{L}{D}\right)_{ls} \tag{50}$$

A 3 2 3

Solving equation (50) for the ballistic entrance velocity yields

$$\frac{V_{E_b}}{V_{sat}} = \frac{3.116}{2.950}\left[\frac{2}{\beta_b \sin\theta_E r_o (L/D)}\right]$$

For typical values of the parameter $\beta_b \sin\theta_E$ for both atmosphere-entry simulators and the earth's atmosphere we obtain required ballistic entrance velocities which are much too small to be practical. Thus simulation of lifting satellite radiation-equilibrium temperatures by ballistic models is not practical.

Ablation

An important quantity to be simulated in an ablation-cooled design is the effectiveness of the ablating material. That is, the amount of heat blockage per unit weight of ablating material. In order that this effectiveness may be duplicated, the mechanism of the type of ablation should be preserved in the scaling process.

Let us consider some simple special cases of ablation to get some general ideas about the mechanism and parameters involved in ablation. We will first assume that the surface has reached a steady-state condition. Radiation effects and effects from chemical reactions will be neglected. This is indeed a simplified model, but it will give us some insight as to the problems that face us.

A heat balance at the surface yields:

$$q = \frac{\dot{m}_L}{A}\left[c_p(T_L - T_o) + L_f\right] + \frac{\dot{m}_L}{A} c_{p_L}(T_v - T_L) + \frac{\dot{m}_v}{A}\left[L_v + c_{p_v}(\overline{T} - T_v)\right] \qquad (51)$$

where q is the heating-rate input and the first term is the heat required to bring the ablating material from some initial temperature T_o to the fusion temperature T_L and convert it to the liquid state. The second term is the heat required to bring the liquid from the fusion temperature to the vaporization temperature T_v. The last term represents the heat required to vaporize part or all of the liquid and to bring the vapor in the boundary layer to some mean boundary-layer temperature, $\overline{T}$. The terms L_f and L_v are the latent heats of fusion and vaporization, respectively. Since this is a steady-state process, the total mass rate of ablation must be equal to the mass rate converted to liquid,

$$\dot{m}_L = \dot{m}$$

It is possible to define an effective heat of ablation for each material as the ratio of the heating rate to a nonablating surface to the mass rate of ablation per unit area, or

$$Q^* = \frac{q_s}{(\dot{m}/A)} = \frac{q_s}{q}\,\frac{q}{(\dot{m}/A)} \qquad (52)$$

This parameter is the critical quantity which must be simulated.

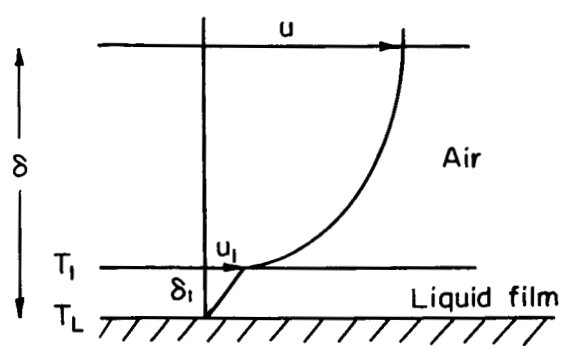

Sketch (d)

No vaporization.- Let us now consider a special case of ablation where only the liquid phase is formed. Sketch (d) shows a model of the boundary layer for this case. For the case of no vaporization, equation (52) may be written as the following:

$$Q^* = \frac{q_s}{q}\left[c_p(T_L - T_o) + L_f + c_{p_L}\left(\frac{T_I - T_L}{2}\right)\right] \qquad (53)$$

Note that a linear temperature profile is assumed in the liquid film.

The basic assumptions which will be made in the analysis of this model will be that $\delta_l \ll \delta$ and that $u_l \ll u$. With these assumptions it can be shown that $q_s/q \sim 1$. Equation (53) can now be written as

$$Q^* = \overline{C} + \frac{c_{p_L}}{2} \Delta T_l$$

where

$$\overline{C} = c_p(T_L - T_o) + L_f$$

$$\Delta T_l = T_l - T_L$$

Let us now see if simulation of this type of ablation is possible in an atmosphere-entry simulator. The model shall be constructed of the same material and shall have the same initial temperature as the full-scale vehicle. Under these conditions, we may write:

$$\frac{Q_m^*}{Q_f^*} = \frac{\overline{C} + \left(c_{p_L}/2\right) \Delta T_{l_m}}{\overline{C} + \left(c_{p_L}/2\right) \Delta T_{l_f}} \tag{54}$$

The conditions which exist in an atmosphere-entry simulator are as follows:

$$\left.\begin{aligned} q_m &= \frac{1}{\lambda} q_f \\ u_m &= u_f \\ Re_m &= Re_f \end{aligned}\right\} \tag{55}$$

Applying Reynold's analogy to the air side of the liquid-air interface

$$h = \rho u c_p \frac{c_f}{2}$$

where c_f is the skin-friction coefficient, and from the conditions given by equation (55) we obtain:

$$c_{f_m} = c_{f_f}$$

It follows that the shear stress at the interface

$$\tau_{l_m} = \frac{1}{\lambda} \tau_{l_f}$$

or

$$\mu_{L_m} \left(\frac{u_l}{\delta_l}\right)_m = \frac{1}{\lambda} \mu_{L_f} \left(\frac{u_l}{\delta_l}\right)_f$$

$$\frac{u_{l_m}}{u_{l_f}} = \frac{1}{\lambda} \frac{\mu_{L_f}}{\mu_{L_m}} \frac{\delta_{l_m}}{\delta_{l_f}} \tag{56}$$

Under the assumption of a very thin liquid film we may write the thin film conduction relation

$$q = \bar{k} \frac{\Delta T_l}{\delta_l}$$

where $\bar{k}$ is the mean conductivity of the liquid film. It follows then, for constant $\bar{k}$, that

$$\frac{\delta_{l_m}}{\delta_{l_f}} = \frac{\bar{k}\, \Delta T_{l_m}}{\bar{k}\, \Delta T_{l_f}} \frac{q_f}{q_m} = \lambda \frac{\Delta T_{l_m}}{\Delta T_{l_f}} \tag{57}$$

Consider now the mass rate of ablation. By continuity it must be equal to the mass which runs off the rear of the vehicle. Therefore we may write the following relation:

$$\frac{(\dot{m}/A)_m}{(\dot{m}/A)_f} = \frac{[\rho_L \delta_l (u_l/2) P]_m}{[\rho_L \delta_l (u_l/2) P]_f} \frac{A_f}{A_m} \tag{58}$$

where P may be thought of as a mean perimeter of the vehicle. Using equations (56) and (57), we may write equation (58) as:

$$\frac{(\dot{m}/A)_m}{(\dot{m}/A)_f} = \frac{\mu_{L_f}}{\mu_{L_m}} \left(\frac{\Delta T_{l_m}}{\Delta T_{l_f}} \right)^2 \tag{59}$$

From the definition of Q^*, we obtain

$$\frac{Q_m^*}{Q_f^*} = \frac{q_m}{q_f} \frac{(\dot{m}/A)_f}{(\dot{m}/A)_m} = \frac{1}{\lambda} \frac{\mu_{L_m}}{\mu_{L_f}} \left(\frac{\Delta T_{l_f}}{\Delta T_{l_m}} \right)^2 \tag{60}$$

Recall, however, from equation (54) that

$$\frac{Q_m^*}{Q_f^*} = \frac{\overline{C} + (c_{p_L}/2)\Delta T_{l_m}}{\overline{C} + (c_{p_L}/2)\Delta T_{l_f}}$$

It then follows that

$$\left(\overline{C} + \frac{c_{p_L}}{2} \Delta T_{l_m} \right) \frac{\Delta T_{l_m}^2}{\mu_{L_m}} = \frac{1}{\lambda} \left(\overline{C} + \frac{c_{p_L}}{2} \Delta T_{l_f} \right) \frac{\Delta T_{l_f}^2}{\mu_{L_f}} \tag{61}$$

For most liquids μ_L is a monotonically decreasing function of temperature; therefore it can be seen from equation (61) that for $\lambda < 1$, $\Delta T_{l_m} > \Delta T_{l_f}$. This, however, means, unfortunately, (from eq. (54)) that $Q_m^*/Q_f^* > 1$, or that not only is exact simulation not probable, but that the degree of simulation is unconservative in the sense that measured mass loss per unit area of the model is smaller than the full-scale value.

It is now proper to inquire how unconservative we are. This question presupposes some knowledge of material properties. Unfortunately, knowledge of the physical properties of many of the ablating materials is indeed lacking. However, a calculation of the effective heat of ablation for a particular material, for which the necessary properties are known, may indicate the order of magnitude of the error in simulation.

Pyrex glass (Corning 7740 glass) was chosen because of the availability of data on its high-temperature properties. The following expression for the viscosity fits the published data quite well (ref. 7).

$$\mu_L = 2.092 \times 10^{-3} \exp\left(\frac{68940}{T_1} - 17\right) \qquad (62)$$

The melting point was taken as $T_L = 3000^\circ$ R. The specific heat of the liquid was taken as 0.33 Btu/lb $^\circ$R, and the constant $\overline{C}$ as 750 Btu/lb. Figure 6 shows, from the solution of equation (61), the liquid film temperature potential of the model versus the temperature potential of the full-scale vehicle for various values of the scale factor. This graph shows that the interfacial temperature difference for the model, ΔT_{l_m}, can become very much larger than the corresponding difference for the full-scale vehicle, ΔT_{l_f}, and hence from equation (57) the inability of properly scaling or compressing the liquid film on the small-scale vehicle. Equations (60) and (62) along with the results shown in figure 6 have been used to calculate the ratio of the effective heat of ablation measured for the model to that of the full-scale vehicle. The results of this calculation are shown in figure 7. Examination of figure 7 shows that if the interface temperature T_1, of the full-scale vehicle, is not too much higher than the melting temperature T_L (say less than 1000° R), the measured Q^* in an atmosphere-entry simulator with a scale factor of say 1/80 is less than 16 percent too high. It also shows that for the same conditions, a larger scale (say $\lambda = 1/10$) rocket-launched test vehicle would simulate full-scale effective heats of ablation to within 10 percent.

It should be noted that this analysis was for ablation in which the liquid phase is present on both the model and the full-scale vehicles. We have shown that the interface temperature of the model can be much higher than that of the full-scale vehicle, so it is possible that although the ablation on the full-scale vehicle consists of only melting, due to the high interface temperature of the model, the ablation on the model may be of the mixed form consisting of both gas and liquid. The applicability of this analysis would then be in question.

Strong vaporization.- Consideration has been given to the case of ablation where only the liquid phase is present. Now consider the other limiting case where all the melt is transformed into vapor or gaseous phase in the boundary layer.

Bethe and Adams (ref. 8) have treated the case of ablation with vaporization and have derived, for the case of a high-viscosity liquid with strong vaporization, the following relation:

$$Q^* = h_V + h_T + 0.68M^{0.26}h_S$$

where h_V is the latent heat of vaporization, h_T is the heat capacity of the vapor, M is the ratio of molecular weights of air to the vapor,

and h_s is the stagnation enthalpy. It can be seen from this equation that Q^* is essentially a function of only the material and the stagnation enthalpy. Therefore if flight velocities are matched, as they are in an atmosphere-entry simulator, it can be expected that measured effective heats of ablation will be the same as will occur on a full-scale vehicle.

Since it has been shown that the effective heat of ablation can be simulated (or at least approximately so) in an atmosphere-entry simulator under the same conditions as were used to simulate thermal stress in ballistic vehicles, the similarity relations for lifting and nonlifting satellites will apply exactly. However, the additional restriction must be imposed that the entrance velocity (hence enthalpy) be the same as that of the full-scale vehicle. This condition restricts the choice of model density scale factor and model scale factor. For models boosted in the earth's atmosphere, some latitude remains in the choice of scale factor by changing the ballistic entrance angle.

Summary of Similarity Relations

In summary, the following table shows, for the types of entries considered, what can be simulated by the techniques discussed in this paper, and which equations govern the choice of model size and weight.

Type of entry	Type of shield	Simulation with -		λ	η
		Boosted models	Simulator models		
Lifting	Heat sink	Yes	Yes	Eq. (37)	Eq. (36)
	Radiation	Yes	No	Any scale	$\eta = 1$
	Ablation	Yes	Yes	Eq. (37)	Eq. (36)
Nonlifting	Heat sink	Yes	Yes	Eq. (44)	Eq. (43)
	Ablation	Yes	Yes	Eq. (44)	Eq. (43)

ILLUSTRATIVE EXAMPLE

In order to illustrate the aforementioned methods of simulation with small-scale models, an example has been worked out below for the case of a simple spherically blunted half-cone configuration. The problem is to use the similarity relations to design small-scale models which can be used to simulate the heating effects due to the atmosphere entry of this vehicle.

The example vehicle is a high-lift, high-drag gliding configuration utilizing a heat-sink design. Figure 8 shows the assumed full-scale dimensions of such a vehicle. Newtonian impact theory gives a lift-drag ratio of 0.87 at an angle of attack of 0°. The lift coefficient referenced to base area is 0.58. For the purposes of this discussion it will be assumed that the vehicle enters the atmosphere along an equilibrium-glide trajectory trimmed at zero angle of attack. The following table gives the assumed parameters of this vehicle.

Area of the base	39.3 sq ft
Plan area	42.9 sq ft
Forward surface area	118.3 sq ft
Volume	111.2 cu ft
Heat-sink weight	1250 lb
Interior capsule weight	2750 lb
Total vehicle weight	4000 lb

It has been shown that simulation of heat-sink thermal stress for this type of vehicle is not possible with a small-scale model of the vehicle. However, simulation is possible by the use of a symmetrical ballistic model (shown in fig. 8) and a proper ballistic trajectory. The problem is to design the model and the trajectory which it follows. We will design two models for this test: (1) a model for testing in the earth's atmosphere, and (2) a model for testing in an atmosphere-entry simulator with $\beta \sin \theta_E = 0.15$ ft^{-1}. In both cases the entrance velocity of the ballistic model will be 18,000 feet per second.

The proper scale factor to be used is determined from equation (37). To test a model of this configuration in the earth's atmosphere ($\beta = 1/22{,}000$ ft^{-1}) assuming an entrance angle of 30° we obtain the required scale factor of $\lambda = 1/11.7$. The scale factor to be used in an atmosphere-entry simulator where $\beta \sin \theta_E = 0.15$ ft^{-1} is $\lambda = 1/952$.

In order to obtain the higher heating rates and shorter times of flight necessary for simulation, we have seen that the over-all density of the model must be increased over that of the full-scale vehicle. Referring to figure 3 or equation (36), we obtain a required model to full-scale density ratio of 7.2. The full-scale over-all density is 36 lb/ft^3, therefore the model must have an over-all density of 259 lb/ft^3. However, one must retain the same material in the heat sink.

All the necessary parameters have now been determined. In conclusion the following table lists these design parameters for the full-scale vehicle and the two models.

	Full scale	Atmosphere test model ($\beta = 1/22{,}000$ ft^{-1})	Simulator test model ($\beta \sin \theta_E = 0.15$ ft^{-1})
Configuration	Blunt half cone	Blunted full cone	Blunted full cone
Entrance velocity	26,000 ft/sec	18,000 ft/sec	18,000 ft/sec
Ballistic entrance angle	---	30°	---
Base diameter	10 ft	10.25 in.	0.125 in.
Over-all density	36 lb/ft^3	259 lb/ft^3	259 lb/ft^3

CONCLUDING REMARKS

It has been found through a motion and heating analysis of various satellite entries (i.e., lifting and nonlifting) that if the heating histories of these vehicles are made dimensionless properly, the heating-rate histories may be represented approximately by the curve for ballistic entries. In this way it was found that one may relate the heating effects on one type of vehicle to those occurring on another and, hence, simulate these effects on a model flying a different type of trajectory.

In particular, it was determined that simulation of thermal stress effects occurring in lifting and nonlifting satellites utilizing a heat-sink design was impossible by simple small-scale tests along similar trajectories. However, it was also shown that simulation of thermal stress effects in lifting and nonlifting satellites is possible by properly designing equivalent ballistic models and testing them along ballistic trajectories. For the case of a lifting satellite, the ballistic model is designed by placing a mirror image of the lower surface of the lifting configuration on top. The concept of altering heating rates and flight times by increasing the over-all density of the model was introduced and similarity relations governing the design of the model were derived.

It has also been shown analytically that it is possible to use an atmosphere-entry simulator designed primarily for the testing of ballistic configurations to test lifting and nonlifting satellite configurations.

Simulation of heating effects on radiation-shield design was also investigated. It was determined that simulation of radiation-equilibrium surface temperatures is possible by a simple scale-model test. Ballistic configurations could not be used because the required entrance velocity of the ballistic model would be too low.

Analysis of two limiting cases of ablation shows that simulation of the effective heats of ablation in an atmosphere-entry simulator is slightly unconservative for the case of liquid ablation and is, within the limits of the assumptions made, nearly exact for the case of ablation with strong vaporization. The conditions of simulation are the same as those for thermal stress simulation.

Ames Research Center
National Aeronautics and Space Administration
Moffett Field, Calif., Nov. 30, 1959

APPENDIX A

NOTATION

A	area, sq ft
B	empirical constant (see eq. (B7))
C	empirical constant, 1.54×10^{-5} slugs$^{1/2}$/ft
C'	vehicle constant (see eq. (10a))
C_1, C_2	constants
C_D	drag coefficient
C_L	lift coefficient
c_f	coefficient of friction
c_p	specific heat at constant pressure
D	drag force, lb
f	transformed altitude coordinate (see eq. (4))
g	acceleration of gravity, ft/sec^2
H	enthalpy
h	heat-transfer coefficient, Btu/ft^2 sec $^\circ$R
K	lifting satellite parameter (see eq. (6))
k	nonlifting satellite parameter (see eq. (18))
$\bar{k}$	mean conductivity of liquid film, Btu/sec ft $^\circ$R
L	lift force, lb
m	mass of vehicle, slugs
$\dot{m}$	mass rate of ablation, slugs/sec
Nu	Nusselt number
Pr	Prandtl number
Q	total heat absorbed, Btu

Q^*	effective heat of ablation, Btu/lb
q	heating rate, Btu/sec ft^2
$\bar{q}$	dimensionless heating rate
r_c	local radius of curvature of flight path
r_o	radius of the earth, ft
T	temperature, ^oR
t	time, sec
$\bar{t}$	dimensionless time
t_o	trajectory time constant, sec
V	vehicle velocity, ft/sec
V_E	velocity of ballistic vehicle at edge of atmosphere, ft/sec
V_{sat}	satellite speed, ft/sec
y	altitude, ft
z	transformed velocity coordinate (see eq. (5))
β	constant, ft^{-1} (1/22,000 ft^{-1} for the earth's atmosphere)
δ	boundary-layer thickness, ft
ϵ	surface emissivity
η	model to vehicle density ratio (density scale factor)
θ	angle of flight path to horizontal, radians
θ_E	entrance angle of ballistic vehicle, radians
λ	model to vehicle scale factor
μ	viscosity, slugs ft^2/sec
ρ	atmospheric density, slugs/ft^3
ρ_o	reference density (0.0017 slugs/ft^3 for the earth's atmosphere)
σ	nose radius, ft
φ	range angle, radians

Subscripts

ı	liquid-air interface (ablation with no vaporization)
b	ballistic vehicle
f	full scale
L	liquid
ls	lifting satellite vehicle
m	model
ns	nonlifting satellite vehicle
s	stagnation
v	vapor

Superscript

*	point of maximum stagnation-point heating rate

APPENDIX B

TURBULENT HEATING RATES

The heating rate is, in general,

$$q = h(T_r - T_w) \tag{B1}$$

where

h heat-transfer coefficient

T_r recovery temperature

T_w wall temperature

or in terms of the Nusselt number (neglecting the wall temperature)

$$q \sim \frac{Nu\ k}{d} T_r \tag{B2}$$

where

d characteristic dimension

k air conductivity

The recovery temperature is approximately (again neglecting the wall temperature) given by

$$T_r \sim \frac{V^2}{2c_p} \tag{B3}$$

Substituting equation (B3) into equation (B2) and introducing the Prandtl number results in:

$$q = \frac{Nu\ \mu_r V^2}{2\ Pr\ d} \tag{B4}$$

The viscosity at recovery temperature can be approximated by

$$\mu_r = C_1 T_r^{1/2} \tag{B5}$$

and the Nusselt number is given empirically by

$$Nu = C_2 (Pr)^s (Re_d)^p \tag{B6}$$

where C_2, s, p are empirical constants. Therefore, if we substitute equations (B3), (B5), and (B6) into equation (B4) and assume a Prandtl number of unity we obtain the heating rate in the following form:

A
3
2
3

$$q = BV^3 \left(\frac{\rho}{d}\right)^p \tag{B7}$$

where B is a constant. Typical values for p for laminar and turbulent flow are 0.5 and 0.8, respectively.

APPENDIX C

SIMULATION OF HIGHLY ELLIPTIC, PARABOLIC, AND HYPERBOLIC ENTRIES

Vehicle Motion and Heating

It can be shown from reference 2 that the trajectory equation for atmosphere grazes from supercircular orbits takes the form

$$f = bF(z) \tag{C1}$$

where b is a vehicle parameter (i.e., function of L/D, type of entry, etc.).

The same arguments advanced for satellite heating-rate histories (see "Heating Analysis") can be used to write the maximum heating rate and vehicle time constant as:

$$q_s^* = CV_{sat}^3 \sqrt[4]{\frac{\beta}{r_o}} \left(\frac{m}{C_D A \sigma}\right)^{1/2} b^{1/2} F^{*(1/2)} e^{(3/2)z^*}$$

$$= CV_{sat}^3 \sqrt[4]{\frac{\beta}{r_o}} \left(\frac{m}{C_D A \sigma}\right)^{1/2} b^{1/2} Q(z^*) \tag{C2}$$

$$t_o = \frac{1}{\sqrt{\beta g}\, b} \int_{z^*}^{z_o} \frac{dz}{F(z) e^{z/2}}$$

$$= \frac{II_o}{\sqrt{\beta g}\, b} \tag{C3}$$

where z^* is determined from

$$\left(\frac{dF}{dz}\right)^* + 3F^* = 0$$

and z_o is such that

$$q_{s_o} = \frac{1}{e} q_s^*$$

on the high velocity side of maximum heating.

Model Motion and Heating

We have seen that simulation of heating effects on ablation-cooled vehicles is obtained if the stagnation enthalpies of the trajectory are duplicated. A convenient method of obtaining these high enthalpies in an atmosphere-entry simulator is to couple a high model launching velocity with a high stream velocity in the simulator nozzle. The high stream velocity in the simulator nozzle (of the order of 16,000 ft/sec) can be obtained by using a shock-heated high-pressure air supply.

The motion equation of a model fired upstream into a supersonic simulator nozzle in a stationary coordinate system along the nozzle center line is then

$$\frac{C_D A}{m} \frac{\rho}{2} (V + V_s)^2 = - \frac{dV}{dt} = V \frac{dV}{dy} \qquad (C4)$$

where

$$\rho = \rho_o e^{-\beta y}$$

and V_s is the stream velocity. Using the coordinate transforms defined by equations (4) and (5) and defining a new coordinate ζ such that $\zeta = z_E - z$, yields

$$\frac{df}{d\zeta} = \frac{\sqrt{\beta r_o}}{(1 + \vartheta e^{\zeta/2})^2} \qquad (C5)$$

where $\vartheta = V_s/V_E$ and where the subscript E refers to the model entrance conditions.

To obtain some gross ideas about the simulation of supercircular entries in such a device and to obtain convenient closed expressions for the solution of equation (C5), the stream velocity will be assumed constant

along the nozzle. As a matter of fact, because of the decrease in static temperature down the nozzle, the stream velocity does remain essentially constant even though the Mach number increases. Integrating equation (C5), using the boundary condition $f = 0$ at $\zeta = 0$ ($z = z_E$), yields:

$$f = \sqrt{\beta r_o}\left(\zeta - 2\ln\frac{1+\vartheta e^{\zeta/2}}{1+\vartheta} + \frac{2}{1+\vartheta e^{\zeta/2}} - \frac{2}{1+\vartheta}\right) \tag{C6}$$

The heating rate to the model is given by equation (9) altered to include the relative velocity.

$$q_s = C\sqrt{\frac{\rho}{\sigma}}\,(V+V_s)^3 \tag{C7}$$

Written in the $f - \zeta$ coordinates, equation (C7) becomes

$$q_s = C''f^{1/2}e^{-(3/2)\zeta}\left(1+\vartheta e^{\zeta/2}\right)^3 \tag{C8}$$

where

$$C'' = CV_E{}^3\sqrt[4]{\frac{\beta}{r_o}}\left(\frac{m}{C_D A\sigma}\right)^{1/2} \tag{C9}$$

Differentiating equation (C8) to determine the f and ζ coordinates of the maximum heating rate yields:

$$\left(\frac{df}{d\zeta}\right)^* - \frac{3f^*}{1+\vartheta e^{\zeta^*/2}} = 0 \tag{C10}$$

Using equations (C5), (C6), (C8), and (C10) we obtain the maximum heating rate as:

$$q_s{}^* = \frac{CV_E{}^3\sqrt{\beta}\,(m/C_D A\sigma)^{1/2}}{\sqrt{3}}\,e^{-(3/2)\zeta^*}\left(1+\vartheta e^{\zeta^*/2}\right)^{5/2}$$

$$= \frac{CV_E{}^3\sqrt{\beta}\,(m/C_D A\sigma)^{1/2}}{\sqrt{3}}\,P(\vartheta,\zeta^*) \tag{C11}$$

Integrating equation (C4) for the time of flight with the boundary condition that $t = 0$ at $\zeta = \zeta^*$ yields:

$$t = \frac{1}{\beta V_E} \int_{\zeta^*}^{\zeta} \frac{e^{\zeta/2} d\zeta}{\left(\frac{f}{\sqrt{\beta r_o}}\right)\left(1 + \vartheta e^{\zeta/2}\right)^2}$$

The vehicle time constant can then be written as:

$$t_o = -\frac{1}{\beta V_E} \int_{\zeta^*}^{\zeta_o} \frac{e^{\zeta/2} d\zeta}{\left(\frac{f}{\sqrt{\beta r_o}}\right)\left(1 + \vartheta e^{\zeta/2}\right)^2}$$

$$= \frac{I_o}{\beta V_E} \qquad \text{(C12)}$$

where ζ_o is such that

$$q_{s_o} = \frac{1}{e} q_s^*$$

where q_{s_o} occurs at $t = -t_o$ on the high velocity side of maximum heating.

Simulation

Matching the maximum heating rates and time constants according to the scaling equations (29) and (30) and defining the density scale factor such that

$$\left(\frac{m}{C_D A \sigma}\right)_m = \eta \left(\frac{m}{C_D A \sigma}\right)_f$$

yields the following similarity equations:

$$\eta = \frac{3Q^2}{P^2} \frac{II_o}{I_o} \frac{1}{(V_E/V_{sat})^5} \qquad (C13)$$

$$\frac{1}{\lambda^2} = \frac{\beta_m}{\sqrt{\beta_f/r_o}} \frac{II_o}{I_o} \frac{V_E/V_{sat}}{b} \qquad (C14)$$

It is now only necessary to evaluate the functions P, Q, I_o, and II_o for the particular entry to be simulated and enough information is obtained to design the simulator model properly.

Parabolic Grazes

Let us examine the particular case of entry from a parabolic trajectory with a subsequent atmospheric skip and energy loss, and exit at circular speed. Equation (C1) takes on the form

$$f = b(z_e - z)z$$

where

$$z_e = \ln 2 \quad (\text{i.e., } V_e = \sqrt{2}\, V_{sat})$$

and b takes on the values (depending on L/D)

L/D	b
-0.5	0.334
0	1.104
.5	3.936

The functions Q and II_o are determined as:

$$Q = 0.658$$

$$II_o = 3.287$$

Figures 9 and 10 show the model design parameters, η (the density scale factor) and λ (the scale factor), versus model entrance velocity for various stream velocities in a simulator nozzle with $^{1}\beta = 0.60$ ft^{-1}. Figure 11 shows how well the heating-rate and enthalpy histories are matched if the design conditions are satisfied.

Also shown in figure 11 are the heating-rate and enthalpy histories for the model resulting from a more refined analysis allowing for the variation of stream velocity down the nozzle. The motion and heating were calculated by a step-by-step integration of equation (C4) with a stream velocity variation as exists in a nozzle with $\beta = 0.60$ ft^{-1}. A value of $(C_D A/m)\rho_o = 0.73$ ft^{-1} was assumed. Notice that although simulation is not accurate on the low velocity side of the heating pulse, it is still possible to match the heating rates and enthalpies adequately up to the maximum heating point.

[1]This is the calibrated value for the Ames small-scale Atmosphere-Entry Simulator.

REFERENCES

1. Eggers, A. J., Jr.: A Method for Simulating the Atmospheric Entry of Long-Range Ballistic Missiles. NACA RM A55I15, 1955.

2. Eggers, A. J., Jr.: The Possibility of a Safe Landing. Ch. 13 of Space Technology. John Wiley and Sons, Inc., 1959.

3. Allen, H. J., and Eggers, A. J., Jr.: A Study of the Motion and Aerodynamic Heating of Missiles Entering the Earth's Atmosphere at High Supersonic Speeds. NACA TN 4047, 1957.

4. Eggers, A. J., Jr., Allen, H. J., and Neice, S. E.: A Comparative Analysis of the Performance of Long-Range Hypervelocity Vehicles. NACA TN 4046, 1957.

5. Chapman, D. R.: An Approximate Analytical Method for Studying Entry Into Planetary Atmospheres. NACA TN 4276, 1958.

6. Sibulkin, M.: Heat Transfer Near the Forward Stagnation Point of a Body of Revolution. Jour. Aero. Sci., vol. 19, no. 8, Aug. 1952, pp. 570-571.

7. Anon.: Properties of Selected Commercial Glasses. Corning Glass Works Bulletin B-83, 1949.

8. Bethe, H. A., and Adams, M. C.: A Theory for the Ablation of Glassy Materials. Rep. 38, AVCO Res. Lab., Nov. 1958.

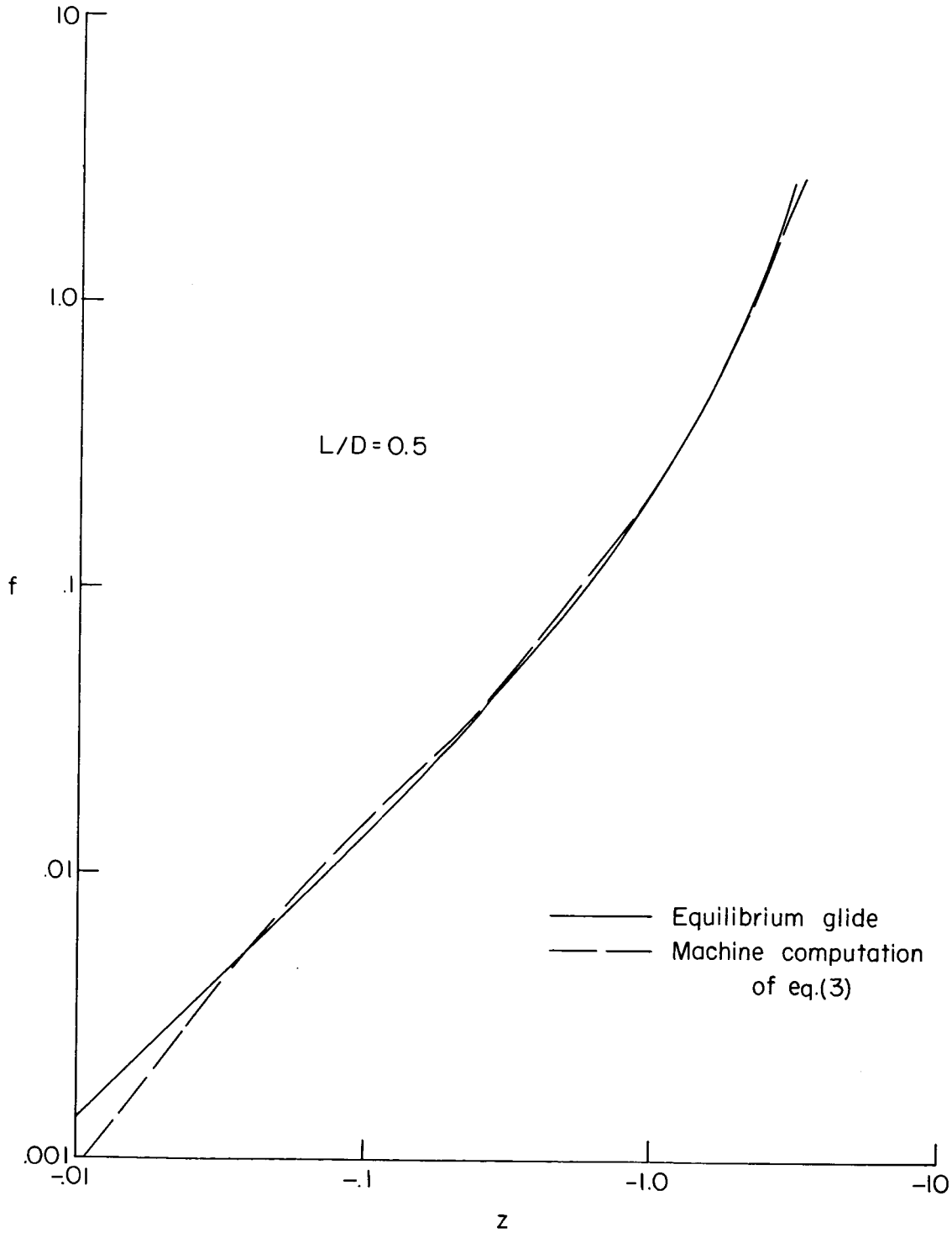

Figure 1.- Comparison of equilibrium glide and machine computations.

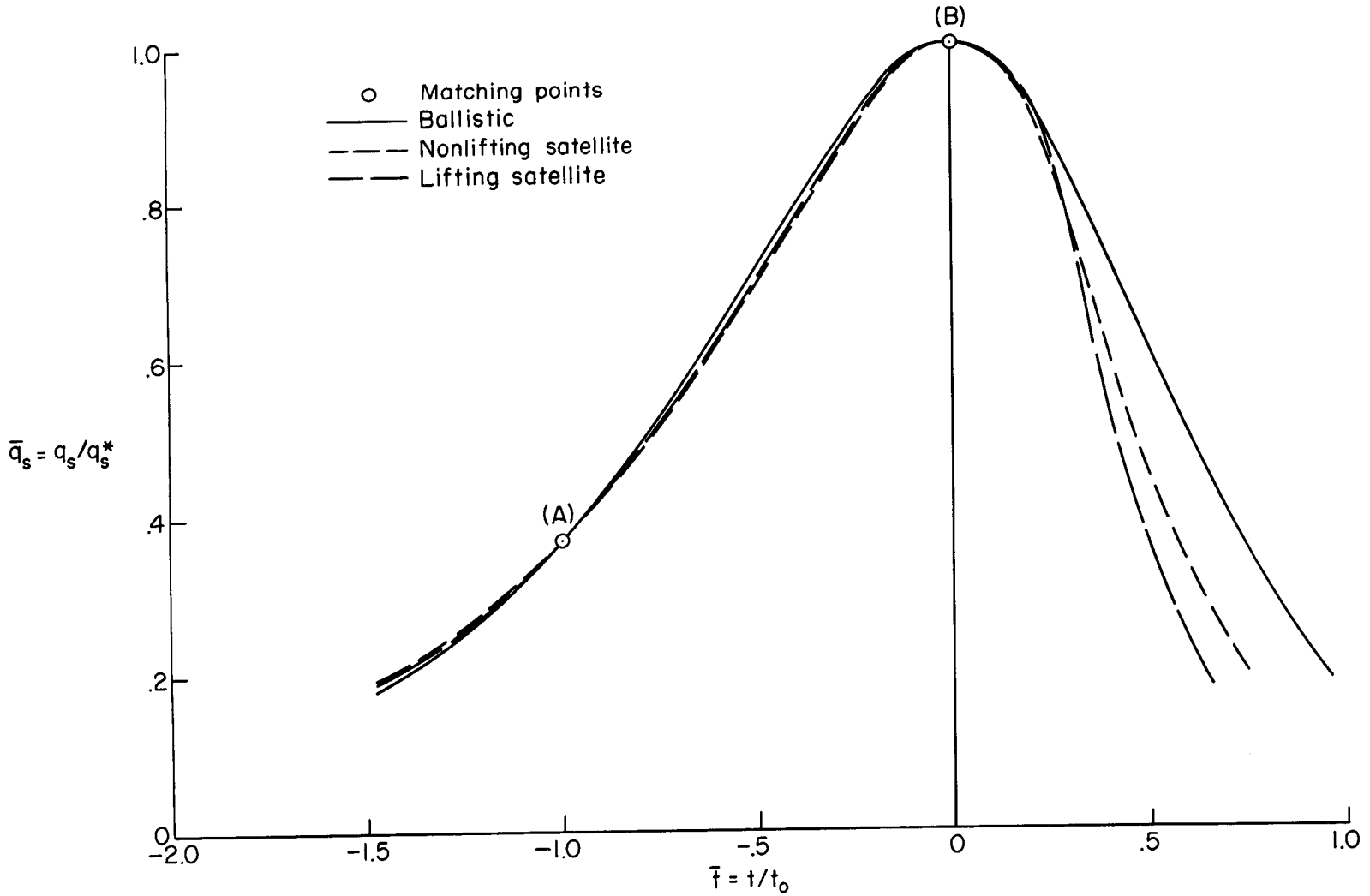

Figure 2.- Dimensionless heating-rate histories.

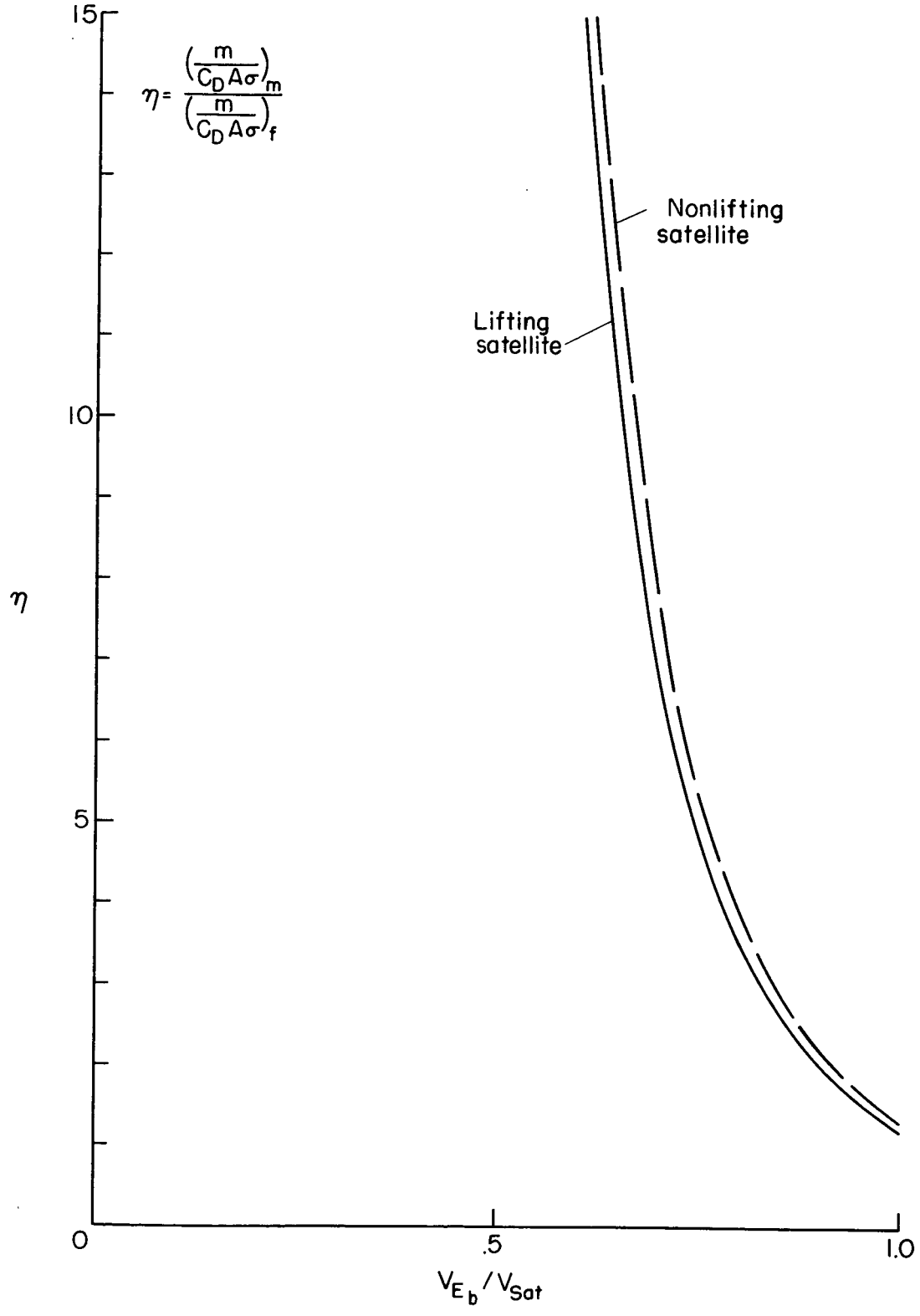

Figure 3.- Density scale factor for the simulation of thermal stress in satellite vehicles.

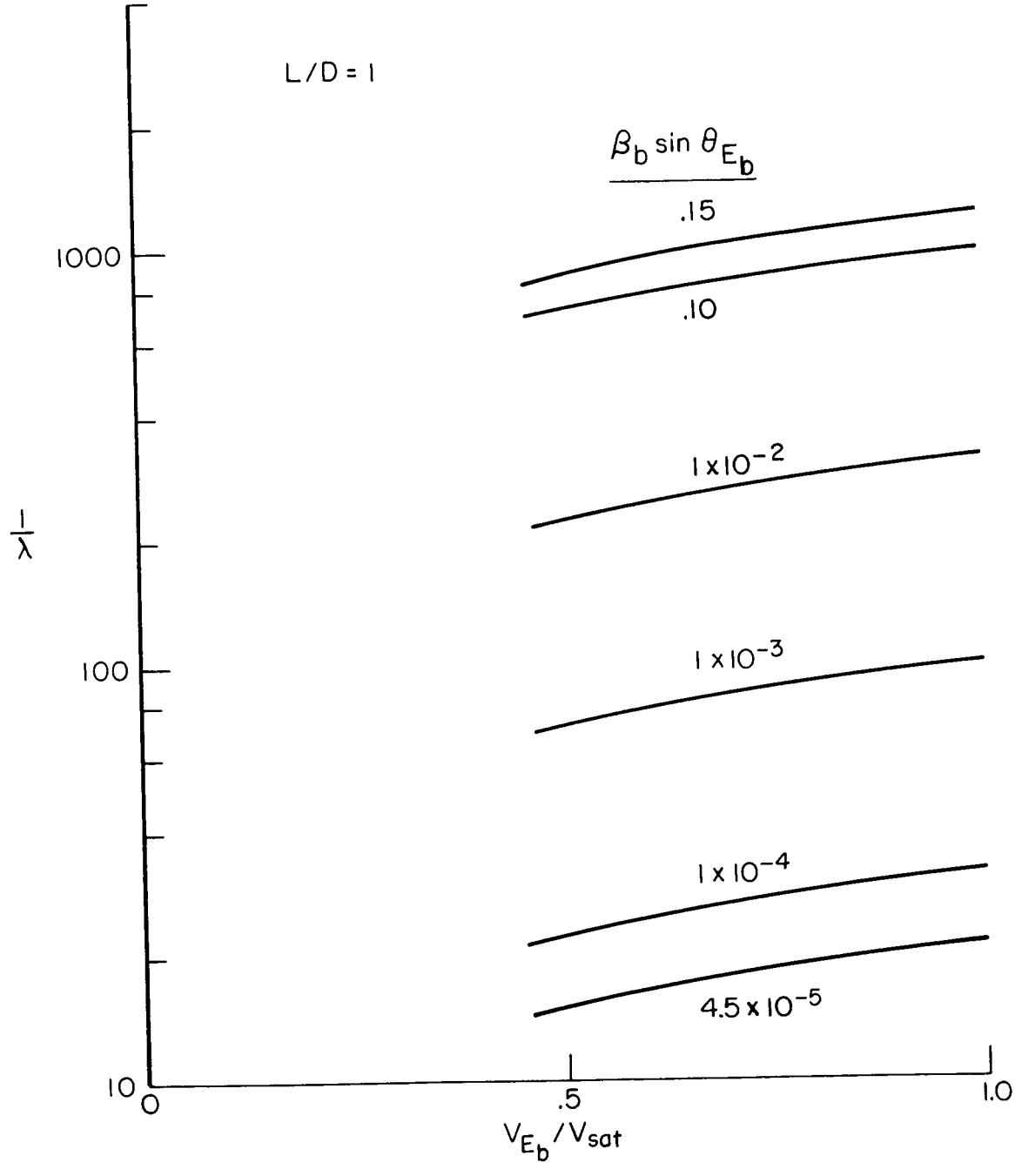

Figure 4.- Scale factor for the simulation of thermal stress in lifting satellites.

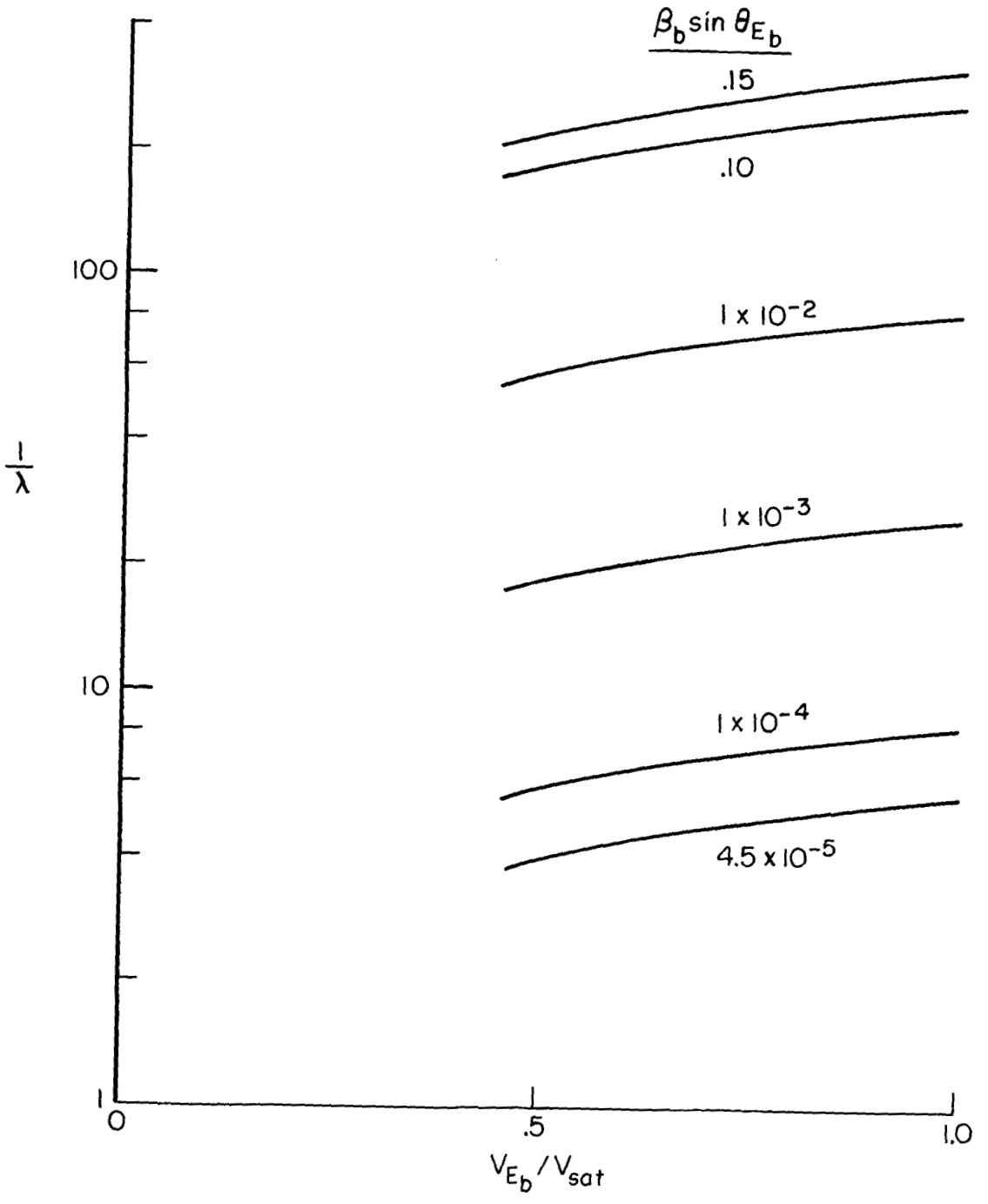

Figure 5.- Scale factor for the simulation of thermal stress in nonlifting satellites.

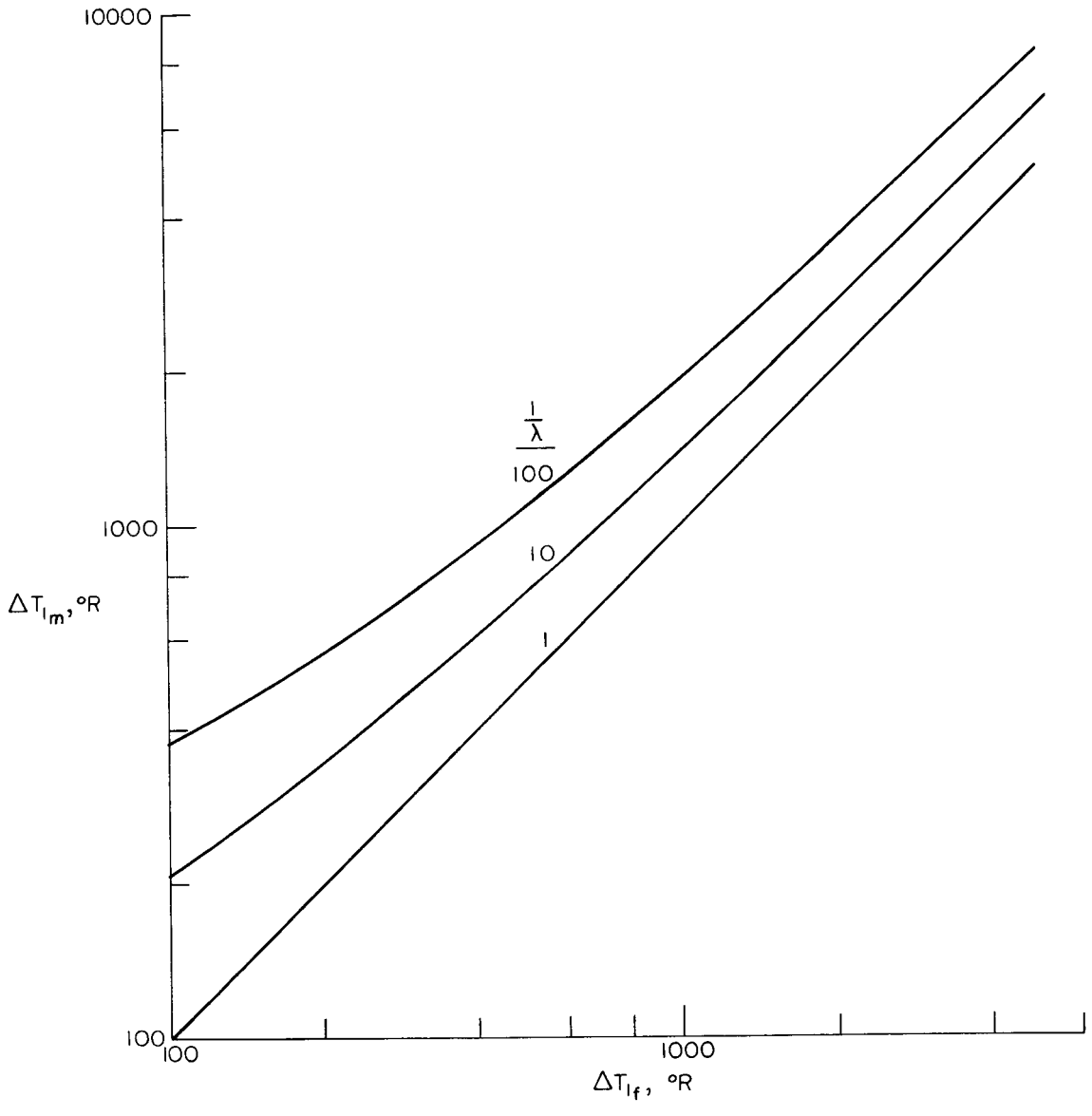

Figure 6.- Model interfacial temperature versus full-scale interfacial temperature.

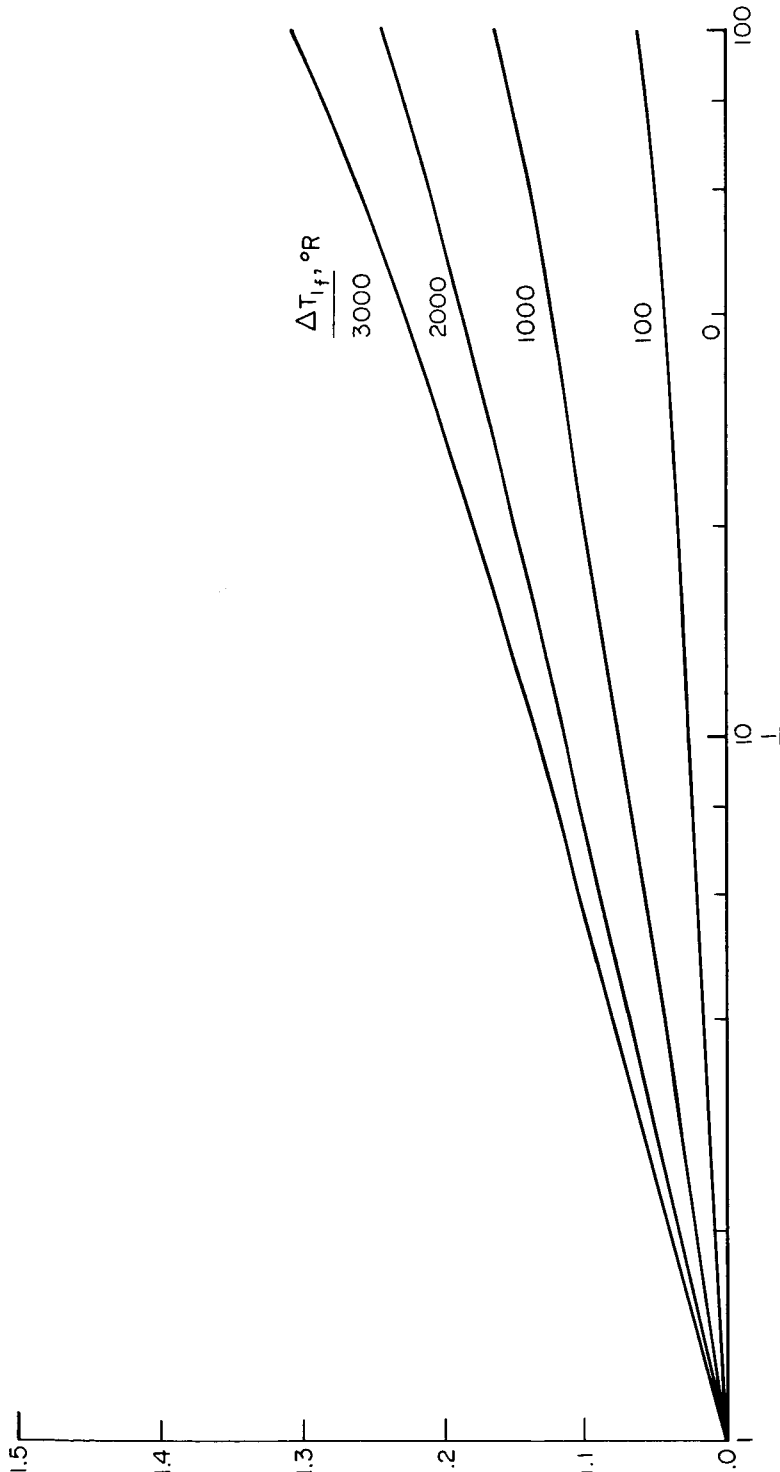

Figure 7.- Comparison of measured and full-scale effective heats of ablation as a function of scale factor.

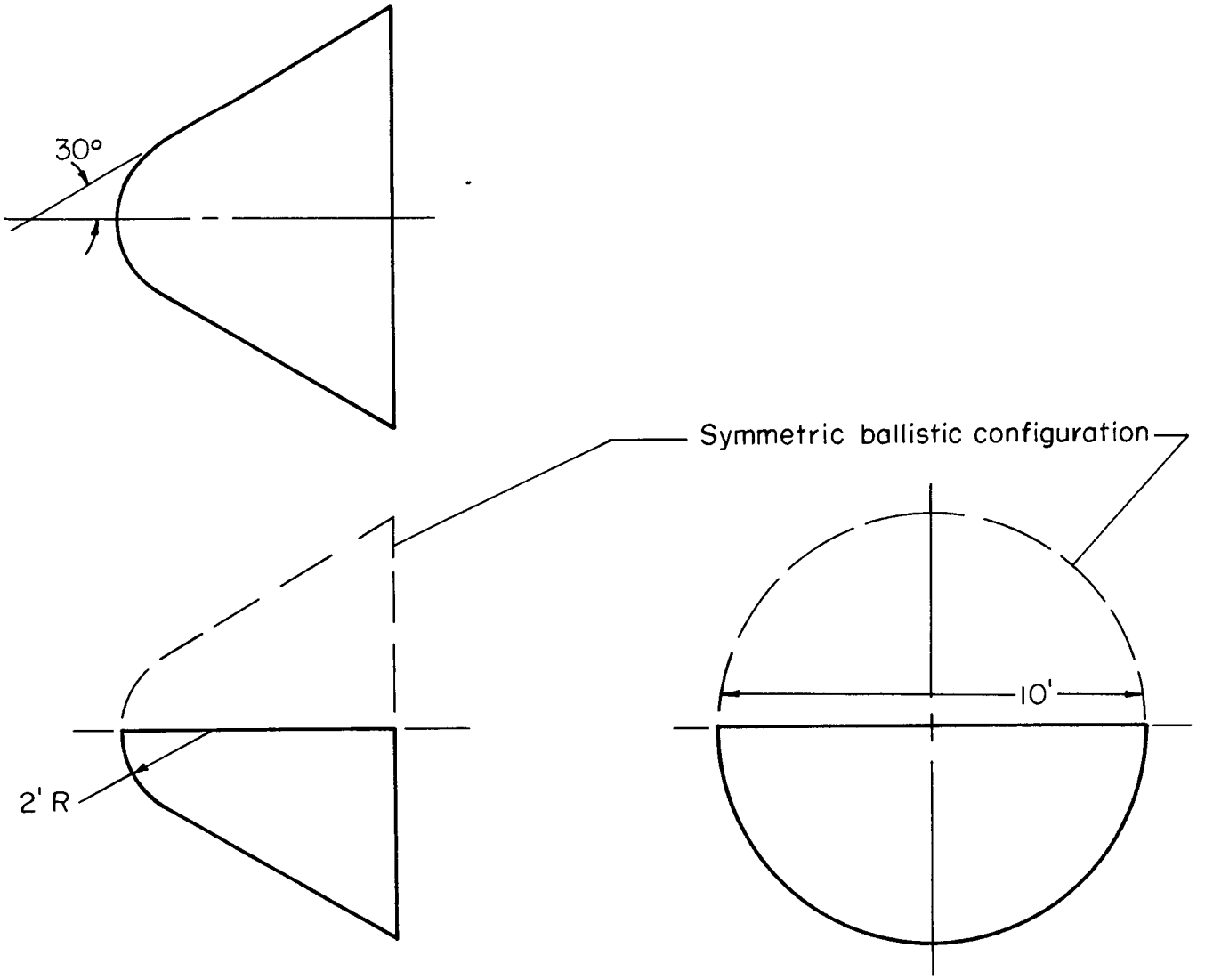

Figure 8.- Example entry vehicle.

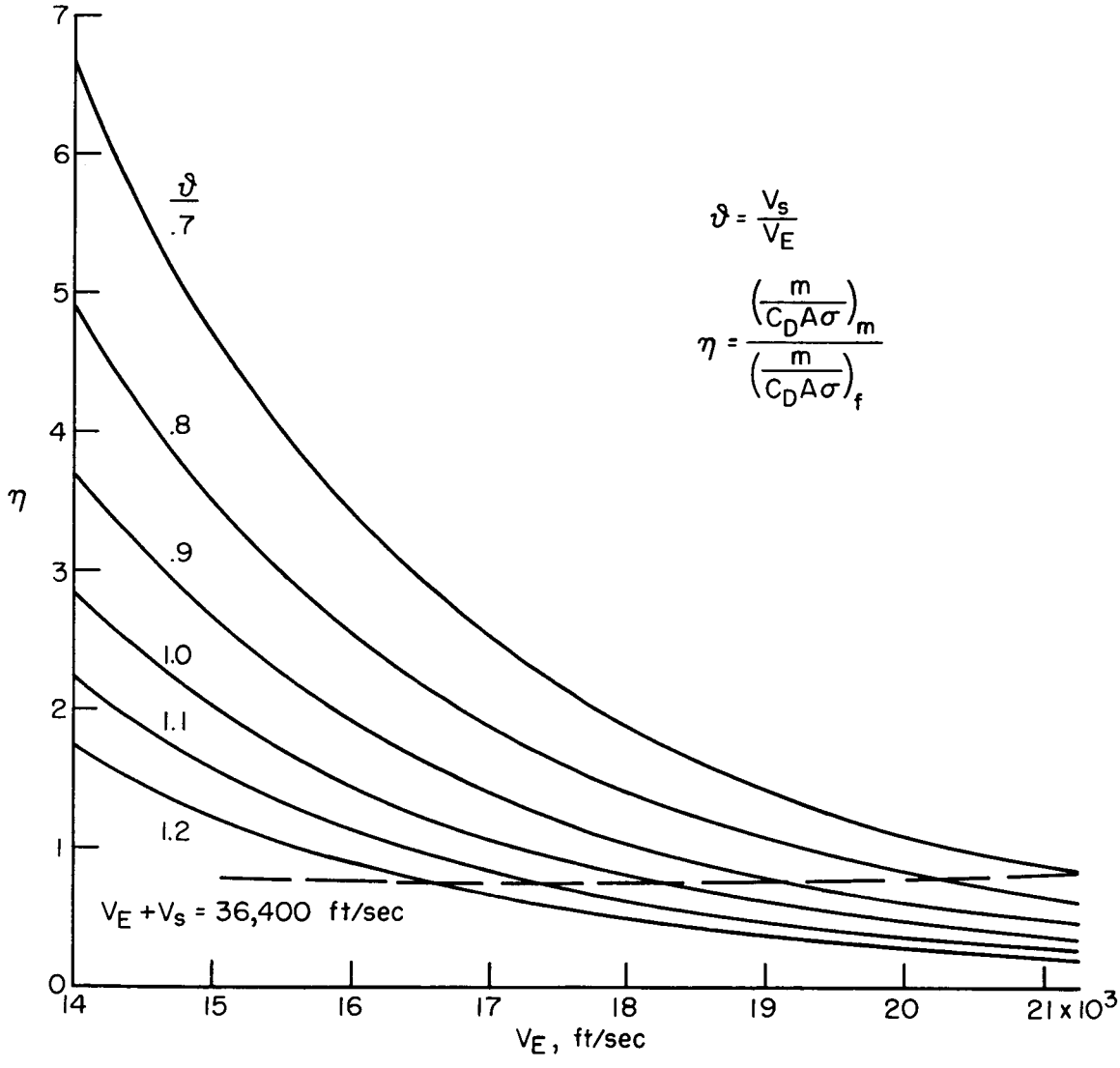

Figure 9.- Density scale factor for the simulation of parabolic grazes (parabolic-entry simulator).

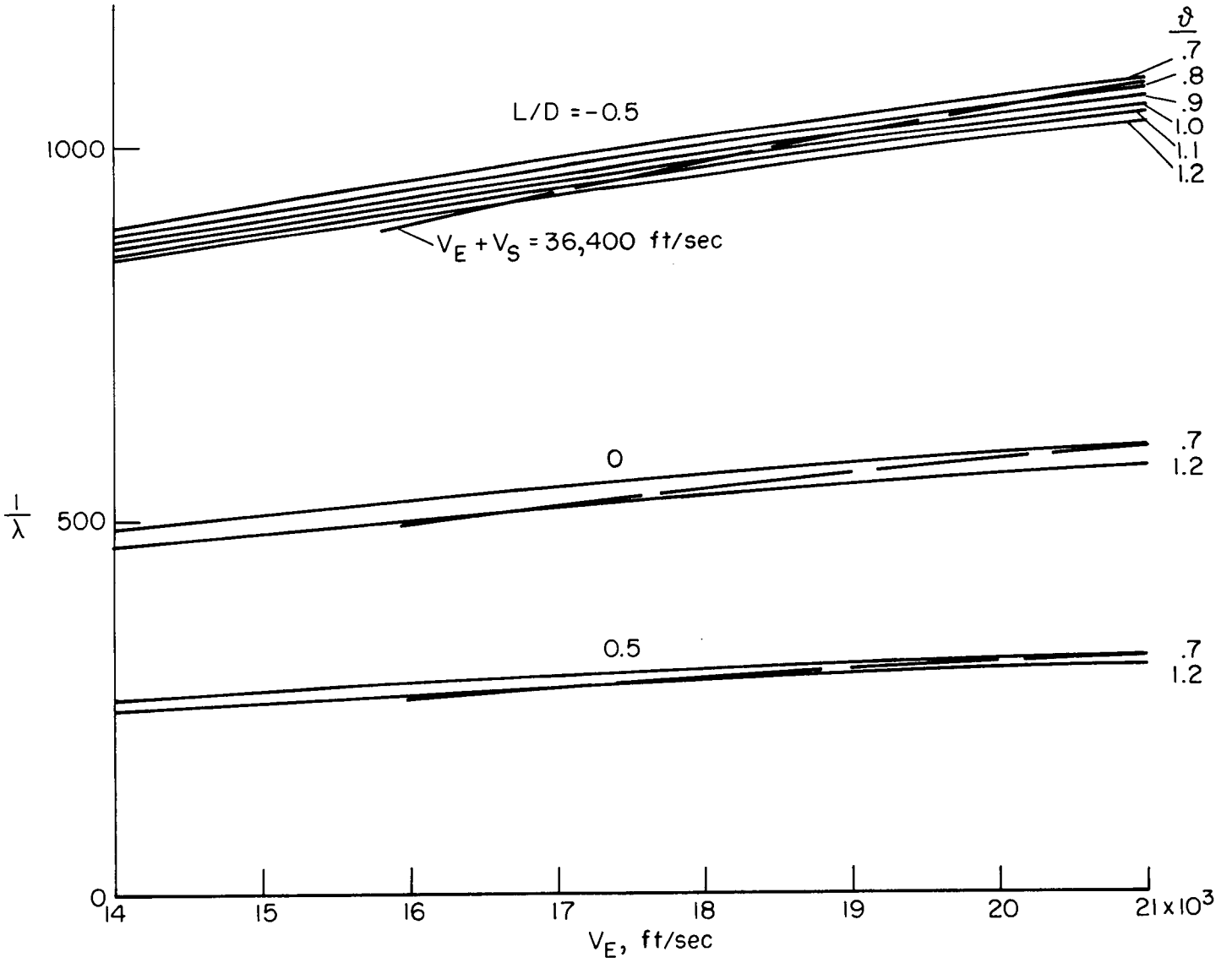

Figure 10.- Scale factor for the simulation of parabolic grazes (parabolic-entry simulator).

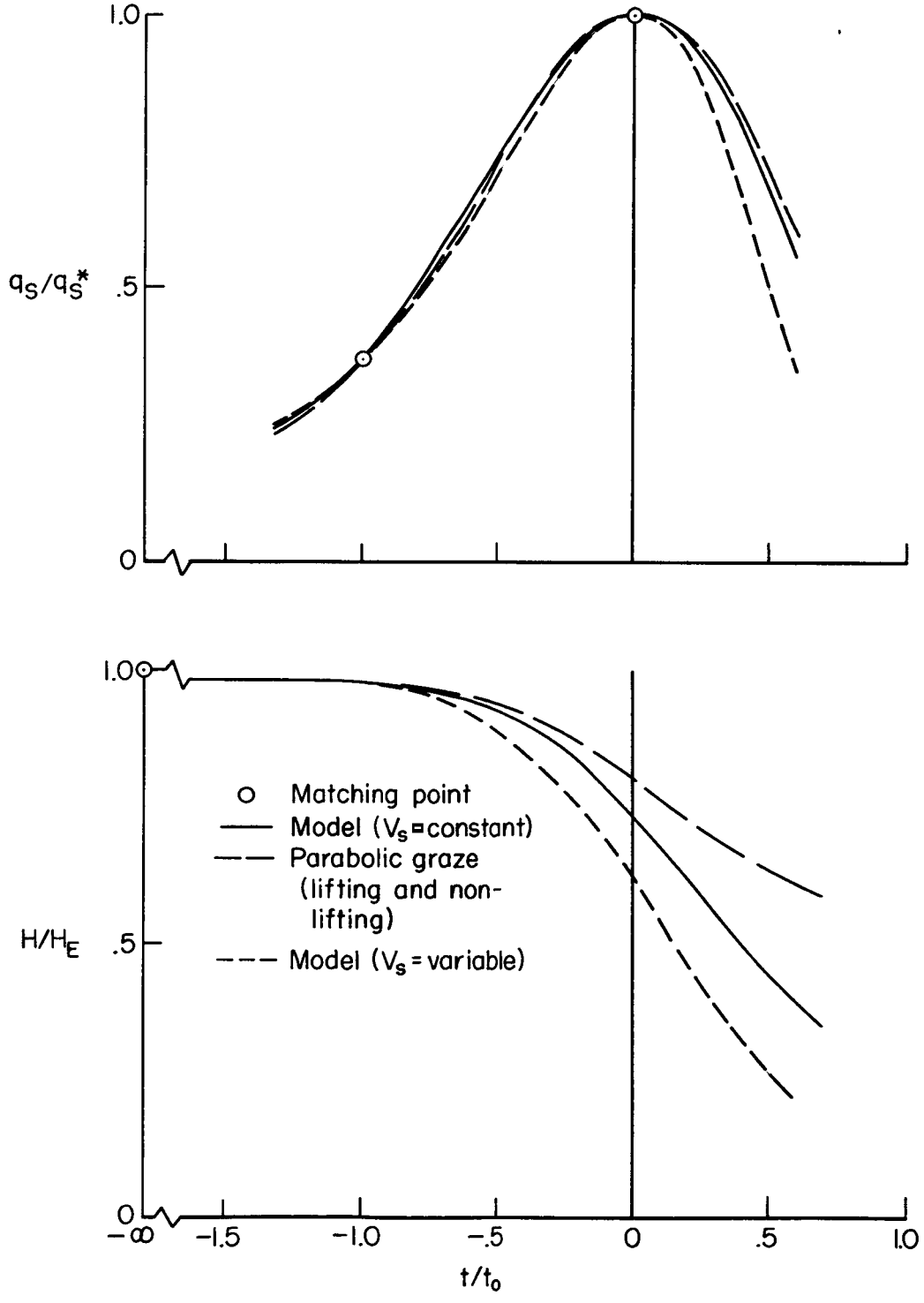

Figure 11.- Model and vehicle heating-rate and enthalpy histories for the simulation of parabolic grazes (parabolic-entry simulator).